Subscale Fast Cookoff Test Results

K. P. Ford, N. C. Davis, A. D. Farmer, E. B. Washburn, A. I. Atwood, K. J. Wilson, J. P. Abshire, M. L Shewmaker, Z. P. Goedert, and C. J. Wheeler
Naval Air Warfare Center Weapons Division, China Lake, California

P. O. Curran
Jacobs Technology Corporation, Ridgecrest, California

J. Covino
Department of Defense Explosives Safety Board, Alexandria, Virginia

ABSTRACT

A controlled-heat-flux device is being developed as a possible alternative to the liquid-fuel-fire test. Six tests were performed assessing the repeatability and scalability of the test article, response of the test article to either a liquid-fuel fire or the controlled-heat-flux device, and the effect of motor internal free space in fast cookoff. Results showed that the reaction times of the test article were very repeatable with differences in time-to-reaction of less than 4 seconds. A test article was cast with a fielded propellant and tested utilizing the controlled-heat-flux device. The controlled-heat-flux device article reacted sooner than a full-scale item with similar energetic material and outside layer thicknesses due to higher temperatures and the more uniform heating found in the controlled-heat-flux device when compared to the full-scale liquid-fuel fire test. The mechanical and thermal responses were very similar for both a liquid-fuel fire and the controlled-heat-flux device. The effect of motor free volume in the fast cookoff test was also examined with the inclusion of a center bore. Results showed earlier times to reaction with the end-burner propellant geometry configuration compared to the test articles with a bore. A modeling effort was undertaken to predict the time-to-reaction of the test assets. This effort was very successful at predicting time-to-reaction with the largest difference between the experimental and the predicted time-to-reaction being 14 percent.

INTRODUCTION

An ordnance item has the potential to be exposed to a fire during its life cycle either during storage and transportation or in theater. The fuel-fire test is a requirement by both the Department of Defense Explosive Safety Board (DDESB) and the Insensitive Munitions (IM) Office in the United States. This test is specified as the external fire test as described in TB 700-2 (Reference 1) for hazards classification relative to transportation and storage, while MIL-STD-2105C (Reference 2) addresses the requirement for operational scenarios with its fast cookoff test. Both of these tests are performed at a system level using STANAG 4240, “Liquid Fuel/External Fire, Munition Test Procedures” (Reference 3). Since these tests occur at the system level, the fuel-fire test is performed late in the development cycle of the munition when it is difficult to make changes should the asset fail. In addition to the difficulty of making changes to correct a failure, the cost of performing a fuel-fire test can be upwards of $1 million for large diameter systems (Reference 4). Due to cost constraints, typically only one or two tests are performed where an inconsistent or conflicting result may occur.

The variability in results is partially due to the liquid-fuel fire itself. Sandia National Laboratory measured the heat flux found in fuel fires to be between 20 and 400 kW/m^2. This variability was found in the same fuel fire; therefore, the location of the item in the fuel fire is important (References 5 through 7). In addition, the top portion of the item is exposed to the greatest heat flux due to the turbulence found in the fuel fire (Reference 8). Fuel fire modeling conducted to understand the critical parameters controlling the reaction response has determined that the factors with the greatest impact on the heat fluxes found in the fuel fire was due to the wind speed as opposed to item location in the fire, diameter of the pool fire, or the pool evaporation rate (Reference 9). Wind is also generated by the fire itself. Variability in wind speed will result in inconsistent heat-flux levels between tests. As a result, test articles may pass in some instances and fail in others.

In an attempt to resolve the variability of the thermal stimulus, the controlled-heat-flux device (CHFD) was designed (References 10 through 13). This device allows the system designer and propellant formulator an opportunity to assess their designs and formulations at the subscale level where changes can be made at relatively low cost. In addition, it also can give the designer an opportunity to see if the design is susceptible to either high- or low-thermal fluxes. The subscale test has the potential to predict how a particular design concept will perform in the full-scale fuel fire. Finally, the liquid fuel/external fire test is being scrutinized with respect to the effect of kerosene-based fuels on the environment (References 14 and 15). The CHFD operates with liquid propane, which is a cleaner burning and more environmentally friendly fuel.

EXPERIMENT

Two experiments were utilized in this study, the liquid-fuel-fire test and the CHFD. The liquid-fuel-fire test consists of a test article suspended 1 meter above a pool filled with JP-8. Instrumentation required consists of four thermocouples (measure the temperature of the fire), two bikini pressure gauges (measure the blast overpressure of the reaction), wind velocity via a anemometer (must be below 5 km/hr or 10 km/hr if using a windshield), audio, and video recordings (audible and visual reactions). A depiction of the test setup and the test article can be seen in Figure 1 and 2. The JP-8 fuel was ignited via a gasoline accelerant at four points. The fire must reach 550ºC within 30 seconds and have an average flame temperature of 800ºC within 2 minutes. The fire will burn for more than 150 percent of the estimated time-to-reaction (Reference 3).

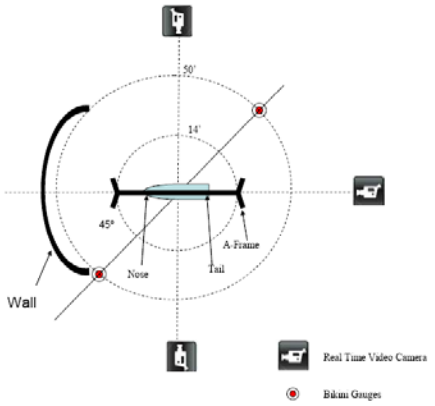

FIGURE 1. Liquid Fuel Fire Test Schematic.

FIGURE 2. Liquid Fuel Fire Test Setup of CHFD Test Article.

The CHFD was designed to provide a uniform, controllable, and reproducible heat flux to the test article (References 10 and 11). The thermal fluxes produced by the CHFD were shown to be similar to those found in fuel fires (Reference 12). The CHFD utilizes a liquid propane/air mixture to obtain the desired heat-flux level. The CHFD is depicted in Figure 3. A fan pushes air through a 5-inch-diameter duct across a propane injector system where the propane/air mixture is then ignited and combusts in the combustion chamber. The test article is located in the disposable chamber area. This disposable chamber area acts as a witness plate to provide a measure of reaction violence. Hydrogen gas is used to ignite the propane/air mixture. Adjustment of the propane/air ratio allows for the change in heat flux. Following ignition, it takes 4 seconds to achieve a steady-state temperature.

The test item is suspended in the disposable chamber via an insertion assembly (Figure 4) throughout the test. The non-disposable section (fan, propane injection area, combustion chamber) is located behind the wall in Figure 4. A graphite flow diverter is located in front of the test article to prevent “hot spot” formation on the impinging surface and produces a more uniform heat flux along the radial surface of the test article (Figure 5). Thermocouple, pressure, and video data are collected along with witness plate and fragment evidence.

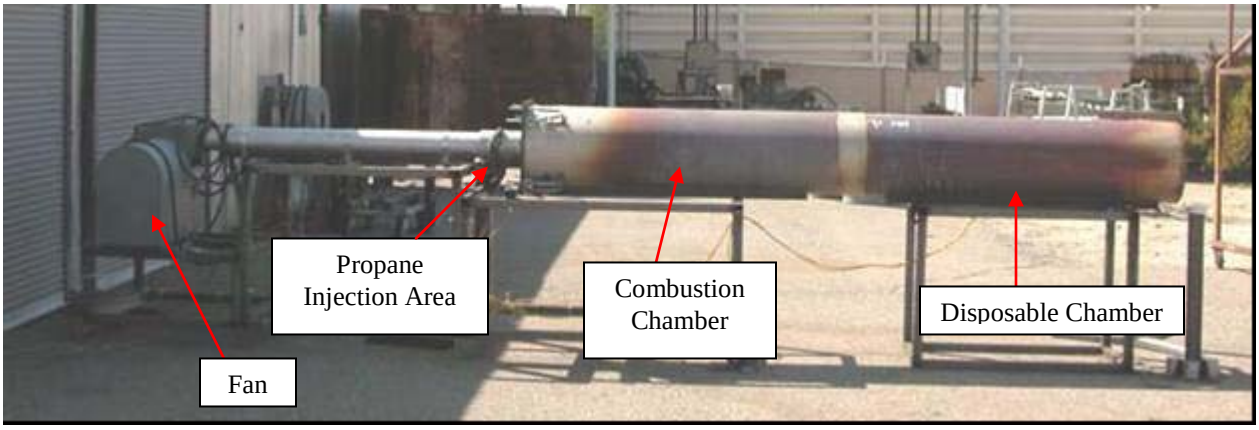

FIGURE 3. Controlled-Heat-Flux Device.

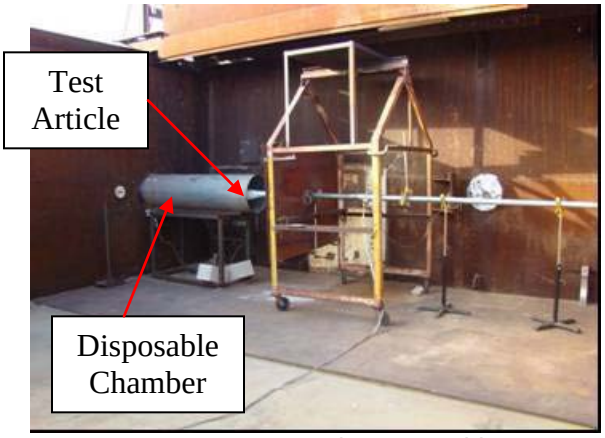

FIGURE 4. Insertion Assembly.

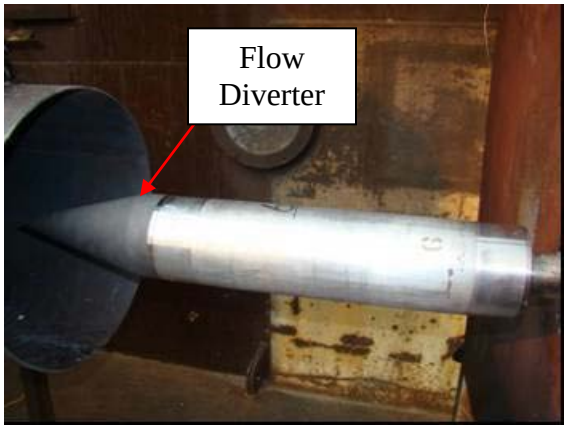

FIGURE 5. Test Article.

The CHFD is currently capable of producing a flux level between 50 to 150 kW/m^2. A calibration device was built that resembles a test article and is capable of measuring the flux levels the test article will experience during the operation of the combustor (Reference 10). The fluxes produced by the CHFD can be reproduced between tests and can be controlled to obtain the desired flux level (Reference 13).

TEST ARTICLE

Two types of test articles were designed to be used in the CHFD. One test article was designed to reproduce the thermal response of a large-diameter solid rocket motor; the other reproduced the thermal response of a tactical rocket motor (Reference 13). The tactical configuration was utilized in the study described in this paper. The case consisted of 4130 steel that had a case thickness of 3.175 mm (0.125 inches) in the propellant area. A 0.762-mm-thick (0.03-inch) ethylene propylene diene monomer (EPDM) was used as the insulation and 0.762-mm-thick (0.03-inch) hydroxyl-terminated polybutadiene (HTPB) with carbon black was used as the liner. Figures 6 and 7 are schematics of the test article. The center section of the test article, 22.86 cm (9 inches) in length, contained the energetic material. All of the test articles examined in this study failed in the center propellant area. The test article also had a center bore to allow for propellant expansion and to mimic tactical motors (Figure 7). High temperature insulation was used on both sides of the propellant to maximize the radial heating.

Thirteen thermocouples were placed in the interior of the test article to measure the heat transfer as a function of time during the test. Thermocouple (TC) 1 and 2 were placed in the forward insulation to record the effectiveness of the insulation/flow diverter. Thermocouples 3 through 11 were placed in the propellant at the liner/propellant interface, with 3 through 5 being on the forward end toward the flow diverter, 6 through 8 in the middle, and 9 through 11 being on the end (aft) closest to the extraction tool.

Thermocouple 12 was located in the center bore of the propellant grain between the forward-middle section and TC 13 was located in the center bore region between the middle-aft section. On each axis, the thermocouples were 120 degrees apart. A low range (6.89 MPa (1,000 psi)) and a high range (68.94 MPa (10,000 psi)) pressure gauge were used to measure the pressure in the bore via 1/8-inch-diameter stainless steel (noted as "PG" in Figure 7).

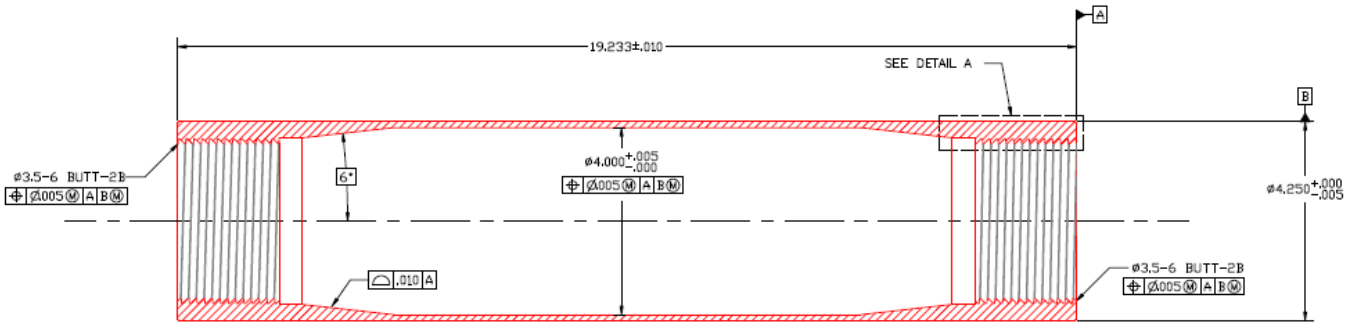

FIGURE 6. Test Article Tactical Configuration.

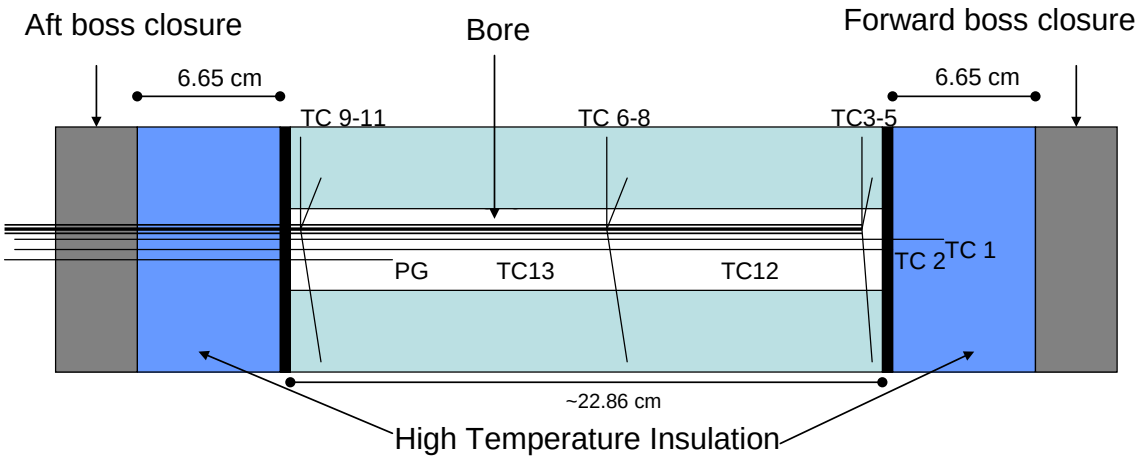

FIGURE 7. Interior of Test Article.

Two energetic-material formulations were examined in this study, a fast burning HD1.3 and a HD1.3 that is currently fielded. Both formulations consist of HTPB binder, bimodal ammonium perchlorate (AP), and aluminum (Al). The fast-burning propellant also has iron oxide, a burning rate catalyst. The fielded propellant includes tetramethylene tetranitramine (HMX). The burning rates of the two energetic materials can be found in Figure 8, with the fast-burning propellant having the highest burning rate at pressures greater than 0.689 MPa (100 psi).

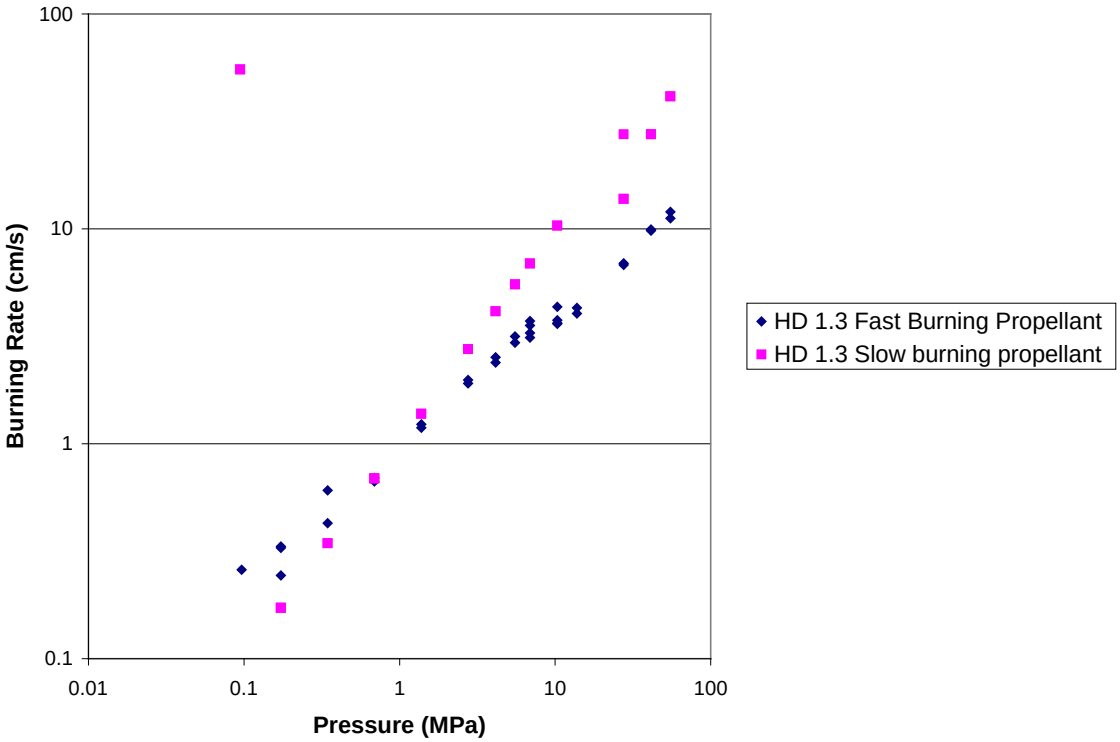

FIGURE 8. Burn Rate Comparison of the Propellant Fills.

APPROACH

Six tests, five tests at 100 kW/m^2 in the CHFD and one test in a liquid-fuel fire, were performed in this study, as shown in Table 1. The reproducibility of the test article was examined using the 3.81-cm bore configuration. The effect of free space (ullage) on the temperature, pressure, and reaction response were examined in this study by looking at the three sizes of bore diameters (end burner (no bore), 1.27 cm (0.5 inch) and 3.81-cm (1.5 inch)). The thermal stimulus' effect on time-to-reaction and case failure was also examined by comparing the results with the same test article from a liquid-fuel-fire test and the CHFD using a 3.81-cm bore geometry. Finally, the ability for the subscale test article to scale to a full-scale asset was also examined. The test article filled with the fielded propellant had very similar thermal properties as the full-scale asset. The time-to-reaction from the CHFD was compared to the full-scale test from a liquid-fuel fire. Two modeling efforts were also undertaken. The first was concentrated on the prediction of time-to-reaction of the five test articles in the CHFD based on the physical and chemical properties of the materials in the test article. The second modeling effort was to begin to quantify the types of reactions produced by the test articles.

TABLE 1. Test Assets Examined in This Study.

Year	Test Asset	Propellant Geometry	Propellant	Test Location
FY08	0	End burner	1.3 fast burning propellant	CHFD
FY09	1	1.27 cm bore		
	2	3.81 cm bore		
	3			
	4		Fielded propellant	
FY10	5		1.3 fast burning propellant	Liquid-fuel fire

THERMOCOUPLE MEASUREMENT DIFFERENCES

During the casting process, the internal thermocouples often moved from their original location either due to the propellant cast or the removal of the mandrel from the motor. Figure 9 is an X-ray of test asset 3 (1.3 fast burning propellant with 3.81-cm bore) showing the final location of the thermocouples following the cast/curing of the propellant. The movement of the thermocouples can cause a wide variation in temperatures that are measured during the test. For example, the thermocouple results for test asset 3 can be found in Figure 10. The thermocouples that are closest to the interface of the liner and propellant show the highest temperatures (TC5, 8, and 11 from Figure 10). As the thermocouple is located farther away from this interface, the temperatures reported are lower due to the insulative properties of the propellant. The temperature in the bore does not increase until near or at reaction (TC1 and 13). Therefore, comparisons in the paper will be based on the highest three thermocouples.

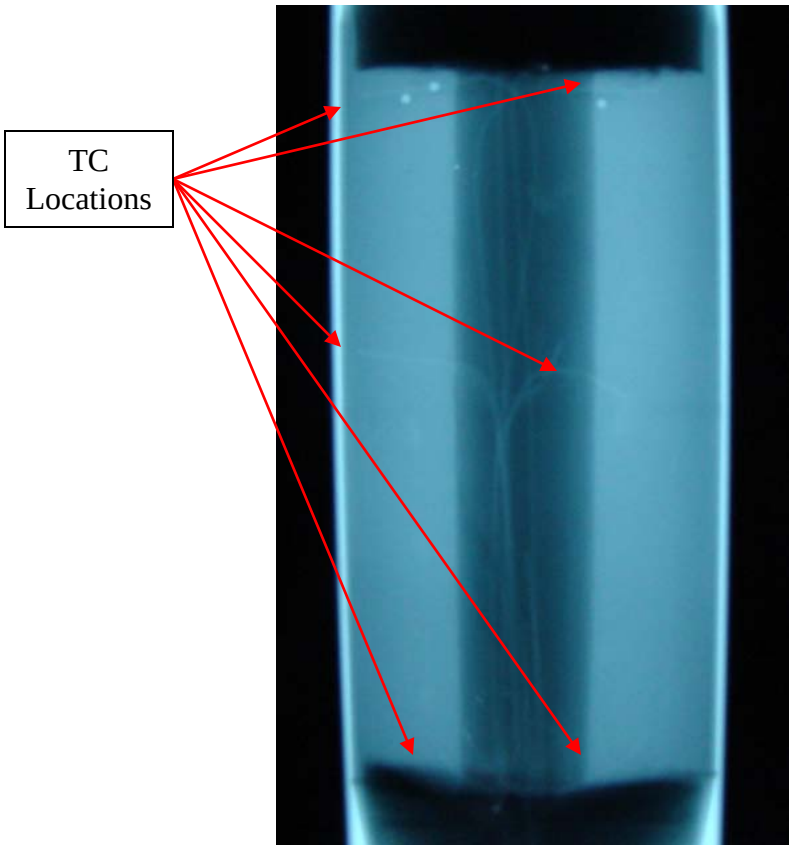

FIGURE 9. X-ray of Test Asset 3 Showing Thermocouple Locations.

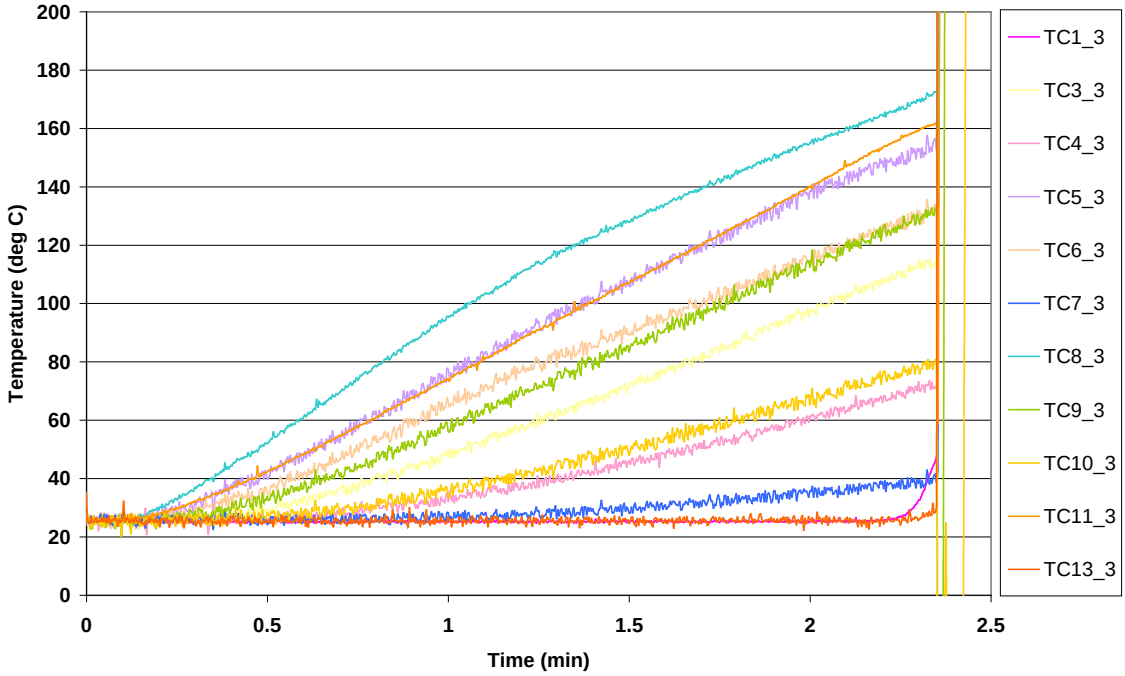

FIGURE 10. Thermocouple Results From Test Asset 3.

RESULTS

REPRODUCIBILITY

Two tests were performed with the 3.81-cm bore test article, filled with the HD 1.3 fast burning propellant, to determine the test reproducibility. Table 2 shows the time-to-reaction of both tests. There is less than a 4-second difference between the two tests. The two test articles also showed similar failure mechanisms in the center of the test asset, with test asset 2 having only three metal fragments (two small fragments located at the top of Figure 11 and one large case fragment) and test asset 3 having four metal fragments (2 small fragments located at the top of Figure 12 and two large case fragments). The graphite flow diverter was not considered as a source of fragments since failure of this section did not damage the witness plate. The three highest temperatures from both tests are plotted in Figure 13. The three highest temperatures from test asset 2 were located at the aft section of the test article, with the highest temperatures recorded from asset 3 being located along the 240-degree axis. The temperatures for asset 3 appear higher than asset 2, which could have possibly led to the difference in fragmentation of the case. However, further study is needed to evaluate whether thermocouple position could account for the difference in temperature.

In terms of repeatability, the CHFD results were very repeatable, especially for time-to-reaction. On the other hand, full-scale testing of an item with similar weight in a liquid-fuel fire showed variability in time-to-reaction in the minutes time regime (0:36 to 5:59 minutes) versus 4 seconds for the CHFD.

TABLE 2. Time-to-reaction of 1.5-inch Bore Geometry.

Test Asset	Propellant Geometry	Propellant	Time-to-reaction, seconds
2	3.81-cm bore	1.3 fast burning propellant	145
3			141

FIGURE 11. Three Metal Fragments Recovered from Test Asset 2.

FIGURE 12. Four Metal Fragments Recovered from Test Asset 3.

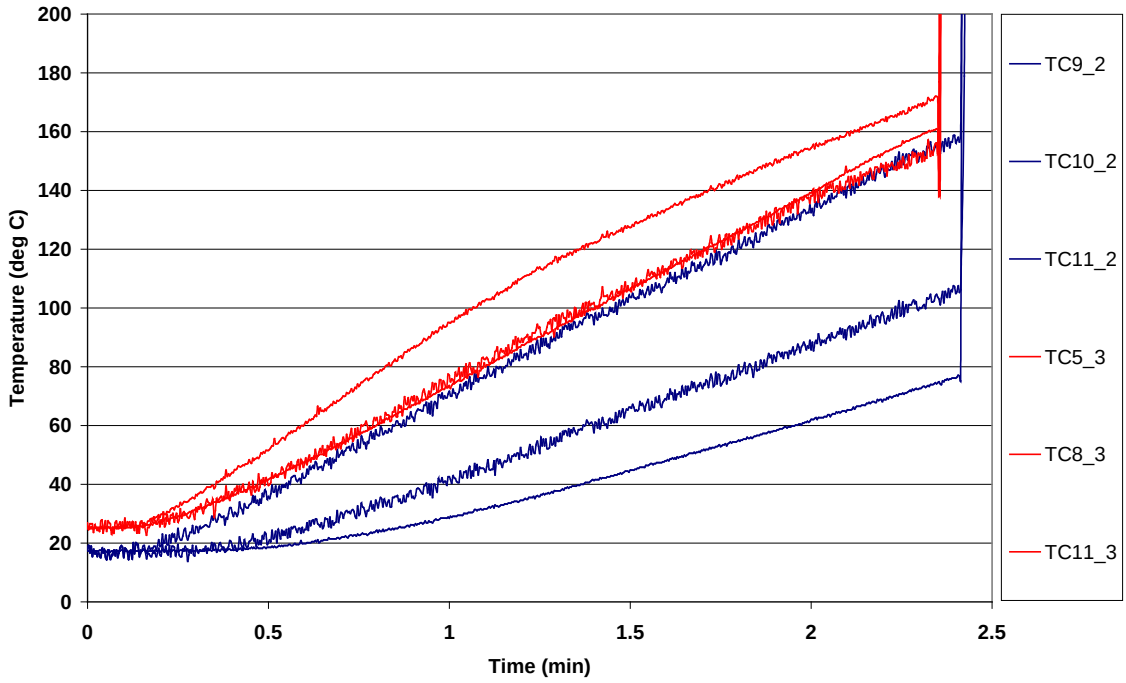

FIGURE 13. Thermocouple Results From 1.5-inch Bore Diameter Tests.

EFFECT OF MOTOR FREE VOLUME

Three bore diameters were examined to assess the effect of bore diameter/ullage on the time-to-reaction or reaction violence in a liquid fuel fire scenario. The bore diameter was varied from 0 to 3.81 cm (0 to 14 percent ullage). The time-to-reaction does seem to be influenced by the bore diameter; however, not enough tests have been done to confirm this statement. In these limited tests, the smaller the bore diameter, the sooner the reaction (Table 3). One possibility may be the creation of the gas bubble in the liner/insulation region, as seen in previous fast cookoff studies. Bubble formation along with the heat intrusion into the propellant causes the grain to expand causing the bore to collapse (Reference 16). The pressure measurement in the bore did not indicate a significant difference between the 1.27- and 3.81-cm bores. This suggests that the majority of the pressure is built up along the interface of the propellant/liner, liner/insulator, or insulator case versus the bore of the motor. The three hottest thermocouples from the 3.81- and 1.27-inch bores, and end burner geometry did not show a large difference in temperature, as shown in Figure 14 (TC data for asset 2 is not shown due to similarity with asset 3, Figure 13). If a hot-spot ignition did not occur at the thermocouple, the thermocouple results would not show the elevated

temperature; and, since the thermal properties of all three types of articles are the same, they should have similar thermal profiles. The case failure for the 1.27-cm bore, shown in Figure 15, produced four fragments similar in number to the 3.81-cm bore (Figures 11 and 12), but the 3.81-cm bore produced smaller fragments compared to the 1.27-cm bore, which could possibly indicate a more violent reaction with the larger bore. Further study is needed to determine if the bore diameter influences the reaction violence.

TABLE 3. Time-to-reaction for 1.3 Fast Burning Propellant.

Test Asset	Propellant Geometry	Propellant	Time-to-reaction, seconds
0	End burner	1.3 fast burning propellant	123.6
1	1.27-cm bore		128.6
2	3.81-cm bore		144.6
3	3.81-cm bore		141.0

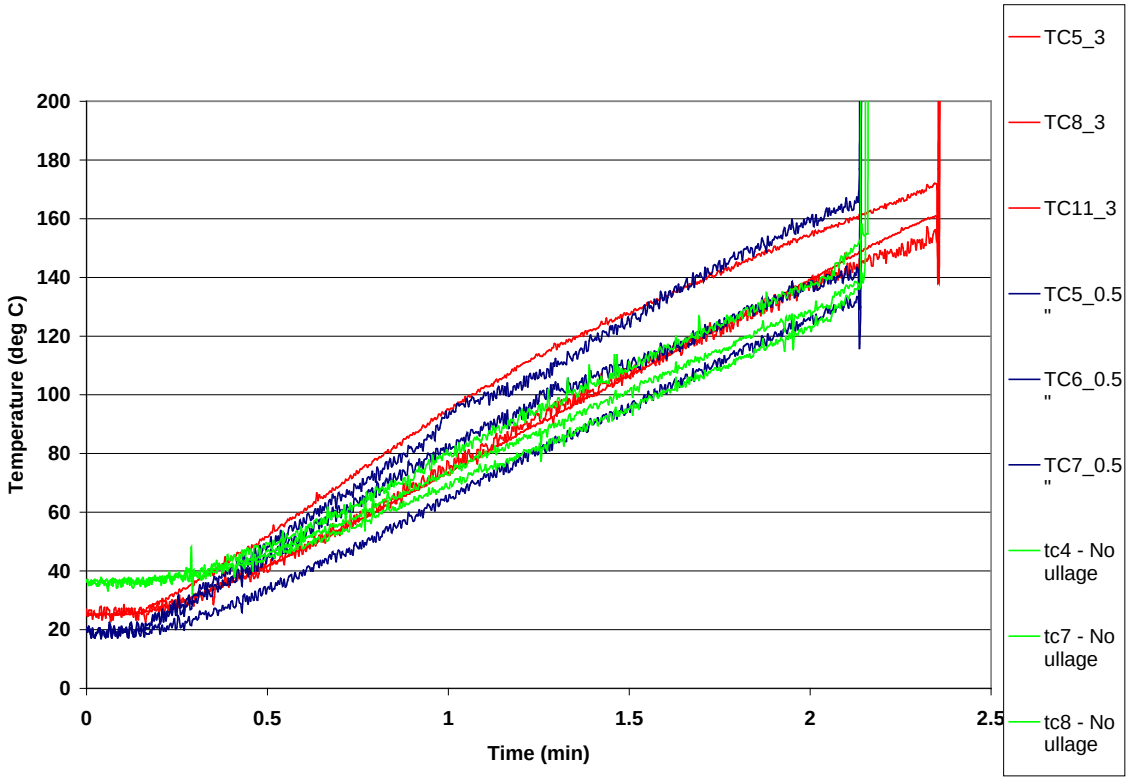

FIGURE 14. Thermocouple Results of Three Hottest Thermocouples Assessing the Effect of Ullage.

FIGURE 15. Four Recovered Metal Fragments from 1.27-cm Bore Diameter.

LIQUID-FUEL FIRE VERSUS CHFD: INFLUENCE OF THERMAL STIMULUS

The test article that has been utilized in the CHFD was also placed in a liquid-fuel fire to compare the effect of the thermal stimulus from the conventional hazard classification test with the proposed new CHFD test methodology. The average flame temperature during the test was 780°C, but varied between 650 to 1100°C, as seen in Figure 16. Figure 17 shows the internal thermocouple temperatures in the test article. Examining the X-rays, the closest thermocouple was 3.175 mm (0.125 inch) from the liner/propellant interface. This offset is attributed to the lower temperature prior to reaction. The test article reacted in 136 seconds. Only three metal fragments were found, two were found in or below the A-frame that held the test article, and the third fragment was located 84 meters (276 feet) from the A-frame. The graphite flow diverter was found within the pool. Figure 18 shows the fragments that were collected. The test would likely be ruled a deflagration due to the distance of the fragments following reaction.

The test article results from the CHFD compare favorably to those from the liquid-fuel fire.

- Similar case failure and fragmentation. Both test articles had failures in the center of the case with a similar number of fragments produced. The CHFD fragments appeared more damaged due to the fragments impacting the witness tube.
- Similar time to ignition. The time to ignition for the CHFD was 5 to 8 seconds later than the liquid-fuel fire, which was unexpected since the temperatures recorded in the liquid-fuel fire were lower than those measured in the CHFD. However, there is significantly more radiation heat transfer in a liquid-fuel fire than in the CHFD, and this could account for the shorter than expected time-to-reaction. Further examination of the video from the liquid-fuel fire showed that a slight breeze caused increased turbulence in the fire as the test asset approached time-to-reaction. This increased turbulence could have caused a hot spot to occur in the motor leading to an earlier time-to-reaction.

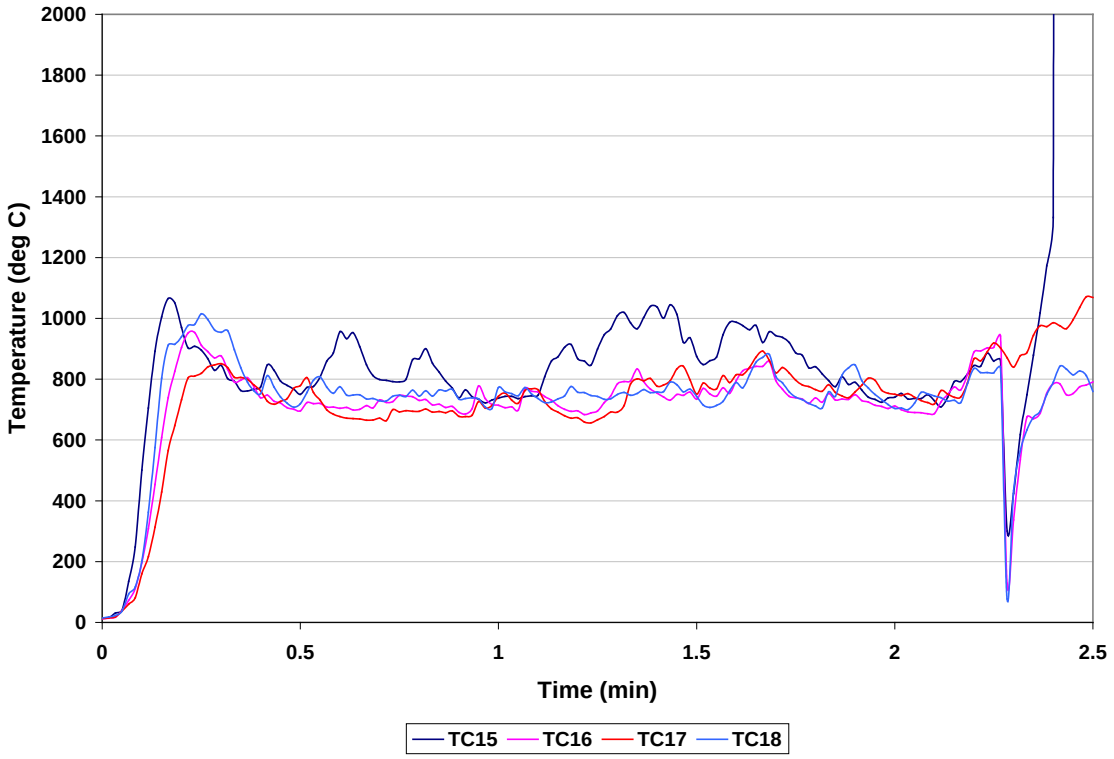

FIGURE 16. Liquid-Fuel Fire Test Setup of CHFD Test Article.

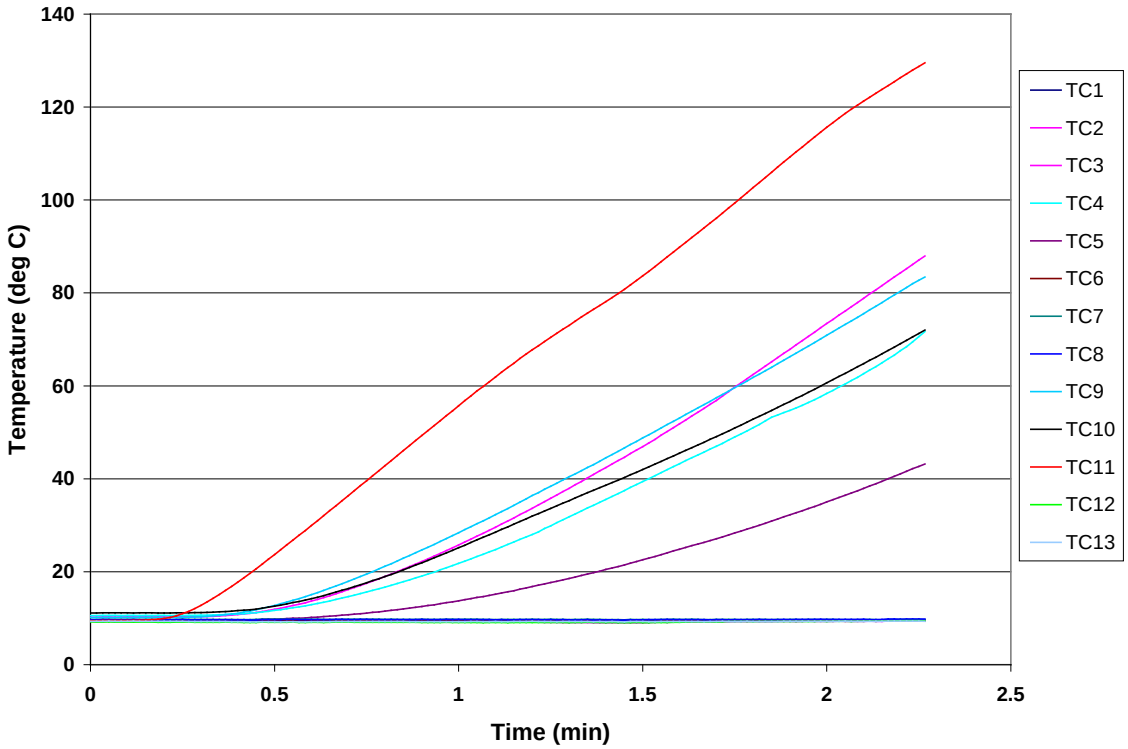

FIGURE 17. Thermocouple Response of CHFD Test Article in Liquid Fuel Fire.

Figure 18. Fragments Collected from Liquid-Fuel Fire Test.

TEST ARTICLE SCALING: VALIDATION OF TEST ARTICLE SCALABILITY

Modeling had shown that matching the thermal properties of the full-scale asset was the most important feature in replicating the full-scale asset's time to ignition (Reference 11). The CHFD article was designed to have similar thermal properties to a full-scale asset that was previously tested in a liquid-fuel fire. Therefore, a fielded propellant with a 3.81-cm bore was tested in the CHFD. The fielded propellant reacted in 126.18 seconds and produced three metal fragments in the CHFD (Figure 19). The thermocouple closest to the propellant/liner interface measured 148ºC at the time of reaction with the bore still at ambient temperature (Figure 20). The system level response from the liquid-fuel-fire test produced a deflagration in 230 seconds (3 minutes 50 seconds). The earlier time to ignition for the CHFD can be attributed to the test article in the CHFD being uniformly exposed to a constant heat flux unlike a liquid-fuel fire that has an extremely variable flux. The liquid-fuel fire also had a lower overall flame temperature, 959ºC, during the liquid-fuel fire test compared to the CHFD, which had a measured temperature of the combusted gases as 1300ºC (1570K) measured at the exit of the disposable chamber. This higher temperature would lead to a higher heat flux into the energetic material that causes the material to react sooner. Thermocouple measurements were also made for the liquid-fuel-fire test; the thermocouples were located in bore and also between the liner and propellant. The highest readings that were measured were 78 and 42ºC at the time of reaction. The temperature in the bore was the ambient temperature at the time of firing (8ºC). These measurements were lower than those measured in the test asset in the CHFD (Figure 20), which is indicative of the lower overall heat flux into the test article during the liquid-fuel fire test.

FIGURE 19. Three Recovered Fragments from 3.81-cm Bore Diameter With Fielded Propellant.

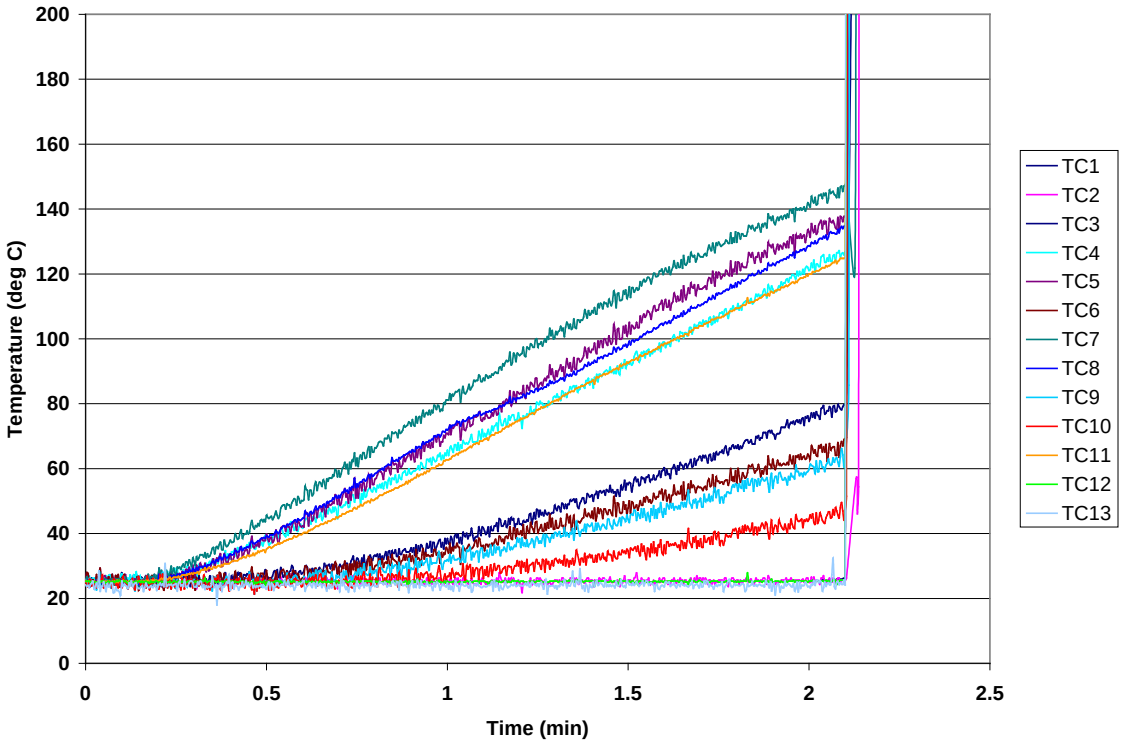

FIGURE 20. Thermocouple Response of Fielded Propellant in CHFD.

MODELING

THERMAL: PREDICTION OF TIME-TO-REACTION UTILIZING COMPUTATIONAL FLUID DYNAMICS

Heat transfer simulations were performed to model heat-flux penetration into the CHFD test article. A two-dimensional axisymmetric model of the test article was simulated in the computational fluid dynamics (CFD) software Fluent, which is depicted in Figure 21.

FIGURE 21. Heat-Transfer Model of Test Article (Not Drawn to Scale).

The model shown in Figure 21 had a case thickness of 0.32 cm (0.13 inch), insulator and liner thicknesses of 0.076 cm (0.030 inch) each, and a propellant thickness of 5.1 cm (2.0 inches). This was done to match the test article dimensions. An axis of symmetry boundary condition was applied to the bottom of the model, while the left and right sides of the model were given zero-flux boundaries. The top of the model had a convective boundary condition. The free-stream temperature was set at 1,570K,

taken empirically from CHFD data. The initial incident power flux was previously measured to be 100 kW/m^2. Fluent has convective boundary conditions that require the free-stream temperature and the heat transfer coefficient. It uses this information to calculate the heat transfer to the boundary. Using the previously measured free-stream temperature of 1,570K, the heat transfer coefficient was changed until the initial power flux to the upper boundary condition was 100 kW/m^2. The final value used for the heat transfer coefficient was 80 W/m^2/K.

Material thermodynamic and transport properties for the insulator, liner, and energetic material used in the heat transfer simulations were measured at the Naval Air Warfare Center Weapons Division (NAWCWD). The physical property values for 4130 steel come from the open literature. The material thermodynamic and transport properties used in the simulations are given in Table 5.

TABLE 5. Material Thermodynamic and Transport Properties.

Material	Density, kg/m^3	Heat Capacity, J/kg/K	Thermal Conductivity, W/m/K
4130 Steel	7,850	298K 477 473K 523 1,073K 837	298K 42.7 573K 40.7 1,473K 30.1
Insulator (EPDM)	1,050	-2,622 + 28.2*T	0.642 + 0.00131*T
Liner (HTBP-based)	1,120	2,680 - 1.93*T	-0.652 + 0.00365*T
Propellant	1,800	6,264 - 29.0*T + 0.0453*T^2	-0.202 + 0.00209*T

The previously mentioned boundary conditions (1570K and 100 kW/m^2) and physical properties of the materials in the test article were applied to the model, and a simulation was run to a simulation time of 400 seconds. A resulting temperature contour plot is shown in Figure 22. The different layers are marked and labeled. The propellant acts as a good insulator, and there is less than a 1 percent difference with the initial temperature 1.6 cm into the propellant.

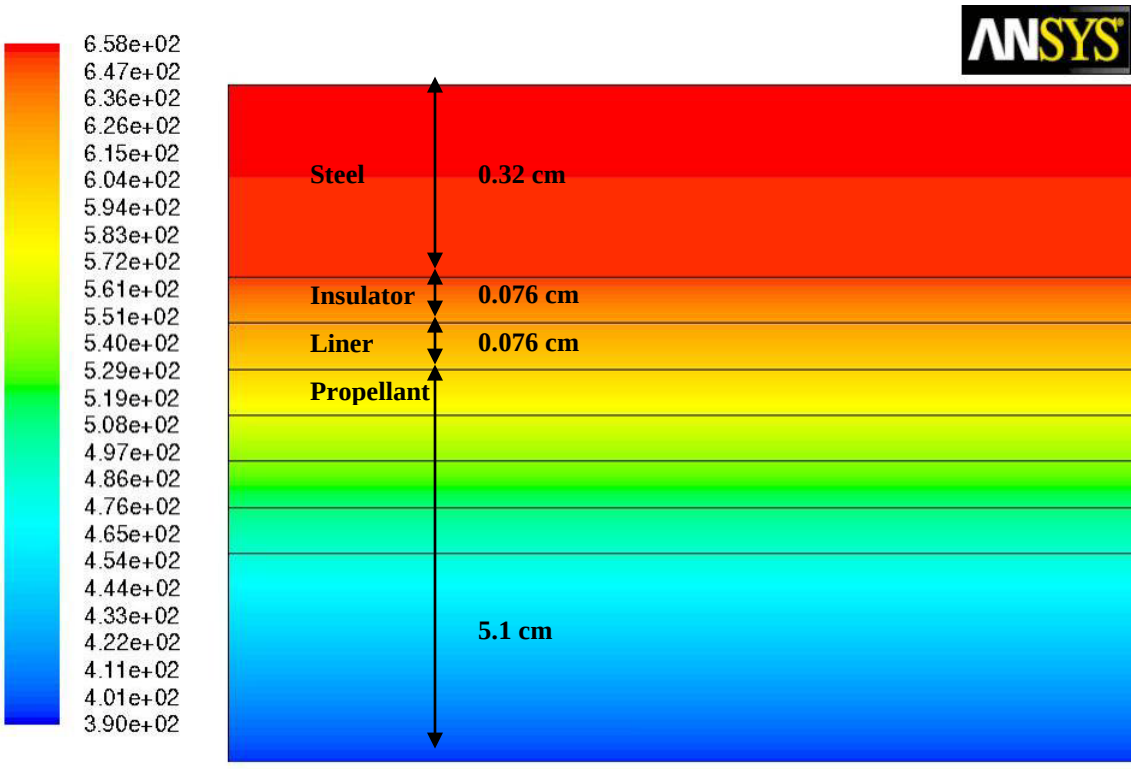

FIGURE 22. Temperature (K) Profile Inside Test Article After 145 Seconds.

An ignition time prediction of the experimental test article using simulation results was desired. A plot of the power flux through the propellant/liner interface is shown in Figure 23 for the test articles with the fast burning propellant (test articles FY08 and 1 through 3).

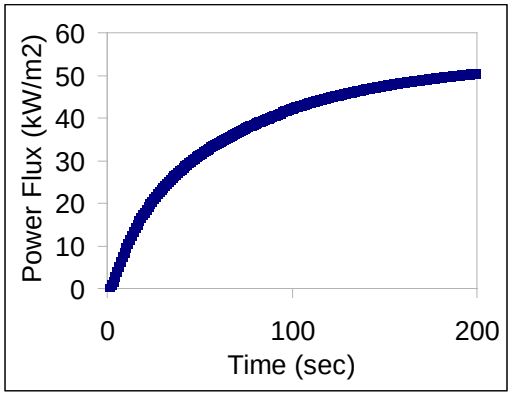

FIGURE 23. Power Flux Into the Propellant at Liner/Propellant Interface.

The simulation calculates the power flux into the propellant and, using experimental time-to-ignition-versus-power-flux data, an ignition time of the test article is predicted. However, the simulated power flux into the propellant is not constant with time while traditional ignition data uses a constant incoming power flux, making direct comparison difficult. Thinking that the total energy flux deposited in a specified time could determine ignition, it was decided to compare the energy flux into the propellant between the simulation and time-to-ignition data. For the experimental data (References 17 through 20), the constant power flux was multiplied by the time to ignition to get the total energy flux that had entered the propellant at ignition. The data points in Figure 24 illustrate this energy flux. The dotted line shows a power fit of the experimental data. To get the solid line in Figure 24, the simulated power flux into the propellant, shown in Figure 23, is integrated with respect to time. Therefore, the simulated energy flux into the propellant represents the total energy flux that has been deposited into the propellant at that time. The region that is to the left of the fit of the experimental data in Figure 24 represents the regime where the propellant has not absorbed enough energy to cause ignition. It was assumed that ignition would occur when the simulated line crossed the experimental data fit. This event occurred at 145 seconds, which was the predicted ignition time of the test article.

Table 6 shows the time-to-reaction for the test assets examined in this study. The largest difference between the predicted and actual ignition times occurred with a 14 percent difference in the end burner propellant geometry. However, the 3.81-cm bore diameters matched the closest to the model with 0.28 percent and 2.76 percent differences in ignition time. Addressing the 14 percent difference, the prediction does not take into account the decomposition of the liner, insulator, and propellant that occurs before ignition. It assumes that the liner and insulator thicknesses are constant and that the heat flux can be modeled as convective with an initial value of 100 kW/m^2. Also, the constant flux time-to-ignition data were taken with similar but different AP/binder/Al formulations. Even with these limitations, the time to ignition predicted was very close to the experimental data. This shows a possible way to use constant power flux time-to-ignition data to predict the time to ignition for hazard situations that do not have a constant power flux.

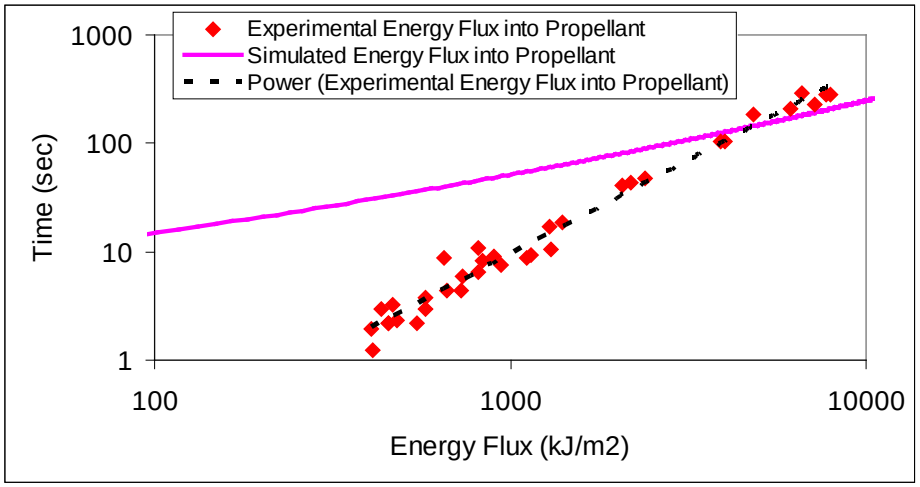

FIGURE 24. Time Versus Energy Flux Into Propellant.

TABLE 6. Time-to-reaction of Test Assets in this Study.

Test Asset	Propellant Geometry	Propellant	Time-to-reaction, seconds	Percent Difference From Model
FY08	End burner	1.3 fast burning propellant	123.6	14.76
1	1.27-cm bore		128.6	11.31
2	3.81-cm bore		144.6	0.28
3	3.81-cm bore		141	2.76
4	3.81-cm bore	Fielded propellant	126.18	12.98

REACTION VIOLENCE

Follow on modeling efforts are to examine the fragmentation of the test article to determine reaction violence by utilizing Sandia National Lab's Presto 3D. The concept consists of determining the kinetic energy of the fragments based on the size of the fragments, distance the fragments are located (if they penetrated the witness tube), and the deformation of the witness tube. This energy will then be correlated with the reaction violence. Items that consistently produced a specific reaction type (detonation, partial detonation, explosion, deflagration, and burn) will need to be tested in the CHFD in order to calibrate the technique. The kinetic energy will be calculated for each of these items providing a basis for separating between reaction types. This concept will then be verified and validated with blind tests.

The current test series produced two to four fragments. These fragments were relatively large and some could easily be tracked to indentations in the witness cylinder. The radial deflection of each indentation was measurable (with an admitted degree of difficulty), allowing for its use as a quantitative measure of impact. A suitable set of fragment and witness cylinder indentation were chosen based on the least amount of deformation while still being a confident match.

The witness cylinder and matched fragment are then modeled in the finite element analysis method (FEM) program Presto from Sandia National Labs. Presto is a 3D, explicit Lagrangian code, with support for the Johnson-Cook strength model to account for material properties over a range of strain rates and temperatures. The fragment is simulated to impact the witness cylinder at a given initial velocity, with the resulting cylinder deformation recorded as output. Figures 25 and 26 demonstrate this concept with the red cylinder segment as the fragment and the blue cylinder segment as the witness plate. The fragment's initial velocity is varied until the calculated cylinder indentation depth matches the measured test data. The calculated initial fragment velocity and mass of the actual fragment can be used together to predict the kinetic energy imparted to the fragment by the energetic reaction during the test event. Predictions

can then be made about the portion of total reaction energy involved in the fragmentation and acceleration of the metal case using heat transfer simulations of the test event. A scaling relationship can then be determined to extrapolate the level of violence to a full-scale hazard test.

Test asset 2 was initially examined using this methodology since it produced three fragments with one fragment providing a clear indication of the impact on the witness tube and the fragment did not show large deformation due to the impact. The modeling of the fragment can be seen in Figures 25 and 26. To provide a dent that matched the impression of the witness tube, the velocity of the fragment upon impact was 38.1 m/s. This produced a total kinetic energy of the fragment as 483 J. The total kinetic energy for each fragment would then be totaled and the sum would be the value for the deflagration (reaction based on liquid fuel fire test).

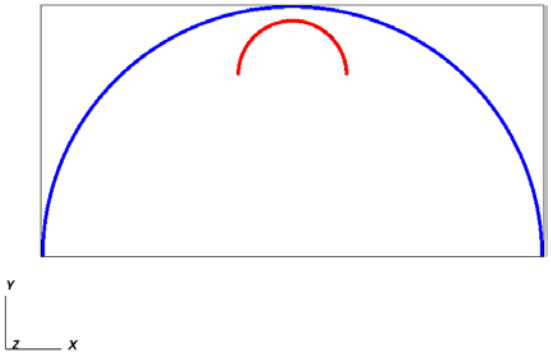

FIGURE 25. Presto Model Prior to Impact of Test Asset 2.

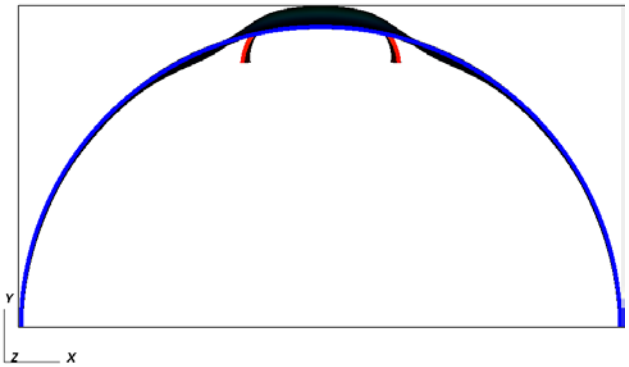

FIGURE 26. Presto Model During Impact of Test Asset 2.

SUMMARY

Six tests were examined in this study utilizing both the CHFD and a liquid-fuel fire. They were performed to assess the repeatability of the CHFD test asset, the effect of free space on reaction time/violence, role of the thermal stimulus on reaction time and reaction violence, and to demonstrate the scalability of the test article to a full scale liquid fuel fire result. The test articles failed in the center with the internal thermocouple responses very dependent on the proximity to the liner/propellant interface and the higher temperatures being the closest to the interface.

- *Reproducibility*. A four second difference between two test articles with a 3.81-cm bore geometry demonstrated the good reproducibility of the test article. Both assets failed in the center and produced three to four metal fragments. The temperature response of the two assets were also very similar, but due to the thermocouple movement during casting one test article showed higher temperatures overall.

- *Effect of Motor Free Volume*. Three motor geometries were examined with varying amounts of ullage (0, 2, and 14 percent). The end-burner geometry reacted first, followed by the 1.27-cm bore, with the 3.81-cm bore geometry reacting last. The thermocouple response was similar for all three geometries. However, the 3.81-cm bore produced smaller fragments compared to the 1.27-cm bore. Further testing and analysis is required to determine the effects of motor free volume in terms of reaction violence.

- *Influence of Thermal Stimulus*. The CHFD test article was tested in both a liquid-fuel fire and the CHFD. The test articles from both types of tests had similar failure mechanisms. However, the liquid-fuel fire had a shorter time-to-reaction even though it was exposed to a lower overall temperature than the CHFD test article. This may have been attributed to increased turbulence in the fuel fire that caused a hot spot to occur leading to an earlier time-to-reaction.

- *Test Article Scaling*. A test article that resembled a fielded system was also tested in the CHFD, and the time-to-ignition results were compared to the time to ignition of the full-scale item in a liquid-fuel fire test. The CHFD asset reacted earlier than the full-scale item. This was due to the thermal stimulus of the fuel fire being less uniform than the CHFD and the flame temperature being lower than the controlled-heat-flux device's gas temperature.

Modeling was used to predict the CHFD time-to-reaction prior to the test. The modeling effort was very successful with the prediction of time-to-reaction at 145 seconds for the fast burning propellant. The test assets reacted between 123.6 seconds to 144.6 seconds. The model utilized a uniform liner and insulator thickness along with time to ignition data for a general AP/HTPB/Al propellant. Radiographs show differences in liner thickness. Taking the variations in the liner and the energetic material's time to ignition could provide a more accurate model.

A method to assess reaction violence for the CHFD was also proposed. This method would be based on both empirical and experimental data. The energy release of the test article would be used to determine reaction violence. This approach would utilize the size of the fragments, impacts in the witness tube, and distance the fragments traveled to calculate the energy produced from the reaction.

FUTURE WORK

Future work for this effort will be focused in four main areas.

- Hazard Response. Adaption of five systems that produced the five types of hazard response (detonation, partial detonation, explosion, deflagration, and burn) to the CHFD test methodology. This will allow for a correlation from the liquid-fuel fire test to the CHFD in terms of reaction response in CHFD.
- Continued Examination of Ullage. Examination of various types of ullage and bores to confirm and probe the reaction response as a result of free space in a fuel fire scenario.
- Validation Testing. Continue evaluation of systems testing in liquid-fuel fires to add fidelity to the CHFD testing methodology.
- Improved Mechanical Response Modeling. Improvement of mechanical response/fragmentation modeling to evaluate and predict reaction violence.

ACKNOWLEDGMENT

This work was funded by the Department of Defense Explosives Safety Board.

REFERENCES

1. *Department of Defense Ammunition and Explosives Hazard Classification Procedures*. TB 700-2 (Army), NAVSEAINST 8020.8C (Navy), TO 11A-1-47 (Air Force), DLAR 8220.1 (Defense Logistic Agency).
2. MIL-STD-2105C, Department of Defense Test Method Standard. "Hazard Assessment Tests for Non-Nuclear Munitions," 14 July 2003.
3. STANAG 4240 ed 2, NATO "Liquid Fuel/External Fire, Munition Test Procedures," 15 April 2003.
4. D.F. Schwartz, T.L. Boggs, and R. R. Bennett. "Costs and Impacts of 1.1 vs. 1.3 Rocket Motors," *Proc of 2003 JANNAF Propulsion Systems Hazards Subcommittee*, December 2003. Colorado Springs, Colorado, CPIA, Laurel, Maryland.
5. M. A. Kramer, M. Greiner, J. A. Koski, C. Lopez, and A. Sou-Anttila. "Measurements of Heat Transfer to a Massive Cylindrical Calorimeter Engulfed in a Circular Pool Fire," Journal of Heat Transfer, 125:110-117, 2003.
6. M. A. Kramer, M. Greiner, J. A. Koski, and C. Lopez. "Uncertainty of Heat Transfer Measurements in an Engulfing Pool Fire," Thermal Measurements: The Foundation of Fire Standards, ASTM STP 1427, American Society for Testing and Materials, West Conshohocken, Pennsylvania, 2001.

7. J. M. Suo-Anttila and L. A. Gritzo. “Thermal Measurements from a Series of Tests with a Large Cylindrical Calorimeter on the Leeward Edge of a JP-8 Pool Fire in Cross-Flow,” SAND 2001-1986, July 2001.

8. J. P. Spinti, E. G. Eddings, P. J. Smith, and A. F. Sarofim. “Heat Transfer to Containers in Pool Fires,” in *Transport Phenomena in Fires,* WIT Press, Southampton, 2006.

9. J.N. Thornock, et.al. “Validation of LES Based Predictions of Heat Flux to Objects in Transportation Fuel Fires,” presented at AFRC/JFRC Meeting, Waikola Beach, Hawaii, 22 October 2007.

10. A. I. Atwood, et al. “Feasibility Studies for Development of an Alternate Test Protocol to the Full-Scale External Fire Test Used in Hazards Classification,” Advances in Energetic Materials and Chemical Propulsion. Begell House, Inc., New York, NY, 2007. Edited by Kenneth Kuo and Juan de Dios Rivera.

11. A. I. Atwood, K. J. Wilson, T. S. Laker, and E. B. Washburn. “Development of a Subscale Fast Cookoff Test,” American Institute of Aeronautics and Astronautics Missile Sciences Conference Naval Post Graduate School, Monterrey, California, 14-16 November 2006.

12. K. P. Ford, et al. "Progress on Development of a Sub-scale Fast Cookoff Test," NDIA Insensitive Munitions & Energetic Materials Technology Symposium, October 2007, Miami, Florida.

13. K. P. Ford, et al. "Sub-scale Fast Cook-Off Testing Results," in proceedings of 2008 DDESB Seminar, Palm Springs, California, August 2008.

14. R.L. Swanson and S. Tanner. “Horizontal and Vertical Integration” presentation at 2008 DDESB Seminar, Palm Springs, California, August 2008.

15. S. Tanner. “Propane as a Surrogate for Kerosene in Fuel Fire Tests” in proceedings of 2010 DDESB Seminar, Portland, Oregon, July 2010.

16. J. E. Cocchiaro. “Subscale Fast Cookoff Testing and Modeling For the Hazard Assessment of Large Rocket Motors,” CPTR72, CPIA March 2001.

17. G. Lengellé, A. Bizot, J. Duterque, J. and Amiot. “Ignition of Solid Propellants,” *Rech. Aerosp.*, Vol. 2, 1991, pp. 1–20.

18. A. D. Baer and N. W. Ryan. “Ignition of Composite Propellants by Low Radiant Fluxes,” *AIAA Journal,* Vol. 3, 1965, pp. 884–889.

19. A. D. Baer, J. A. Keller, and N. W. Ryan. “Ignition of Ammonium Perchlorate Composite Propellants by Convective Heating,” *AIAA Journal,* Vol. 4, 1966, pp. 1358–1365.

20. A. I. Atwood, K. P. Ford, D. T. Bui, P. O. Curran, and T. Lyle. "Radiant Ignition Studies of Ammonium Perchlorate Based Propellants," 2nd European Conference for Aerospace Sciences (EUCASS) Brussels, Belgium, July 2007. (Also to be published in EUCASS Book Series, Advances in Aerospace Sciences, Vol. 1 - Propulsion Physics, March 2008.)